

The effect of volumetric and out-of-phase cyclic loading on strain accumulation

T. Wichtmann, A. Niemunis & Th. Triantafyllidis

Institute of Soil Mechanics and Foundation Engineering, Ruhr-University Bochum

ABSTRACT: The process of strain accumulation under cyclic loading is influenced not only by the average state of stress, the void ratio and the magnitude of the amplitude. The shape of the strain path during a cycle, i.e. its openness and polarization is of crucial importance. In this paper cyclic triaxial tests with a simultaneous variation of the vertical and horizontal stress components during cyclic loading are documented. The results demonstrate that not only the deviatoric part of the strain loop governs the accumulation but also the volumetric part significantly contributes. Furthermore, test results from a novel cyclic multiaxial direct simple shear (CMDSS) device are presented. It is shown that circular strain paths produce higher accumulation rates in comparison with one-dimensional ones. A change of strain polarization during cyclic loading leads also to an increase of the accumulation rate (of temporary nature). A possible consideration of the observed effects in an explicit constitutive model is outlined.

1 INTRODUCTION

The importance of cumulative effects in soils under cyclic loading is undisputable, Wichtmann et al. (2004). The influence of the average stress σ^{av} , the void ratio e and the magnitude of the strain amplitude ϵ^{ampl} on the accumulation rate was demonstrated using cyclic triaxial tests.

In earlier works (e.g. Niemunis et al. 2003) we assumed that the volumetric portion of the strain path during a cycle can be completely disregarded. This assumption was based on the work of Ko & Scott (1967), who studied the effect of isotropic stress cycles on the accumulation of strain in cubical sand samples. The isotropic stress cycles resulted in purely volumetric strain loops with no further accumulation except for the first cycles. Thus, the volumetric part of the strain path was excluded from our procedure of calculating the multiaxial amplitude \mathbf{A}_ϵ (Niemunis 2003, Niemunis et al. 2004).

In the meantime we have checked this assumption. For this purpose cyclic triaxial tests with a simultaneous variation of the vertical stress σ_1 and the lateral stress σ_3 have been performed and are documented in this paper. Different inclinations of the stress path α (see Fig. 1) and thus strain paths of varying polarization (i.e. with different ratios of deviatoric and volumetric portions) were studied. Contrarily to our earlier assumption a significant contribution of the volu-

metric part of the strain loop has been observed.

Several researchers reported an influence of the shape of the strain loop (Pyke et al. 1975, Seed et al. 1978, Ishihara & Yamazaki 1980, Boulanger & Seed 1995) or a change of strain polarization during cyclic loading (Yamada & Ishihara 1982) on the accumulation process. This paper documents also tests using a novel cyclic multiaxial direct simple shear (CMDSS) device. The accumulation due to OOP strain paths (circular shearing) was compared with the residual strain of IP paths (shearing in one direction). The tests show that a circular cyclic shearing produces approximately twice larger accumulation rates compared to a one-dimensional shearing. Moreover, a sudden change of the direction of shearing (i.e. the polarization of the strain amplitude) leads to a temporary increase of the accumulation rate.

The notation presented in Section 2 of Wichtmann et al. (2004) is also used within this paper.

2 CYCLIC TRIAXIAL TESTS WITH CONTROL OF σ_1 AND σ_3

The cyclic triaxial device presented in Figure 3 of Wichtmann et al. (2004) has been modified in order to vary the vertical and the lateral stresses simultaneously. The vertical force was applied by a pneumatic loading system while the cell pressure was varied by

a pressure control valve.

Four test series were performed so far. Similar initial densities were used in all tests. In the first test series samples were cyclically loaded at an identical average stress σ^{av} with equal deviatoric stress amplitudes q^{ampl} while the isotropic stress amplitude p^{ampl} was varied resulting in different stress path inclinations α . In a second series of tests pure isotropic stress loops of identical amplitude p^{ampl} were applied to the specimens at different average stress ratios η^{av} but identical average mean pressure p^{av} . Both series exhibited a significant influence of the volumetric part of the strain loop on accumulation. The third test series is an attempt to quantify the contribution of the deviatoric and the volumetric portion of the strain loop to the accumulation rate. For this purpose different inclinations α and different amplitudes were tested while the average stress σ^{av} was kept constant. In the fourth test series ellipsoidal stress paths in the $p - q$ - plane were applied.

All specimens were prepared by dry pluviation and then fully saturated. The tests were performed on medium coarse sand (the grain size distribution curve is shown in Figure 4 in Wichtmann et al. 2004). 10,000 cycles with a frequency of 0.05 Hz were applied to the specimens in all tests. The low frequency of 0.05 Hz was chosen due to reliable operation of the pressure valve regulating σ_3 in this range.

2.1 Tests with identical deviatoric and variable isotropic stress amplitude

Specimens were prepared with similar initial densities ($0.58 \leq I_{D0} \leq 0.59$), consolidated under an identical average stress ($p^{\text{av}} = 200$ kPa, $\eta^{\text{av}} = 0.75$) and cyclically loaded. While the deviatoric part of the stress amplitude $q^{\text{ampl}} = 60$ kPa was held constant the isotropic amplitude p^{ampl} was varied, i.e. different stress path inclinations α ($45^\circ, 60^\circ, 71.6^\circ$, see Fig. 1) were used. The inclination $\alpha = 71.6^\circ$ corresponds to $\sigma_3 = \text{const}$.

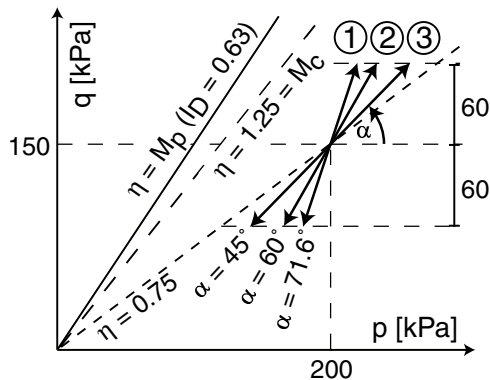


Figure 1. Stress paths in the $p - q$ - plane in tests with identical deviatoric but different volumetric part of the cyclic stress path

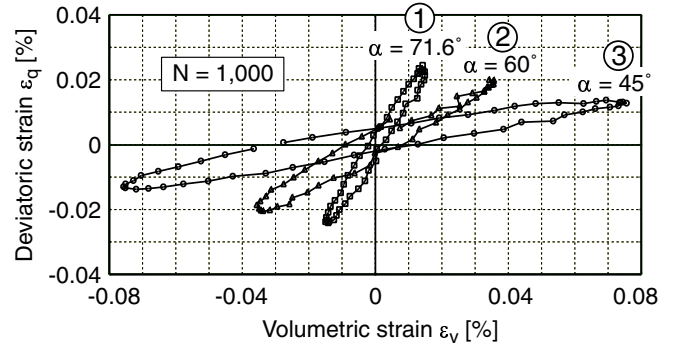


Figure 2. Strain loops in the $\epsilon_q - \epsilon_v$ - plane in tests with identical deviatoric but different volumetric part of the cyclic stress path

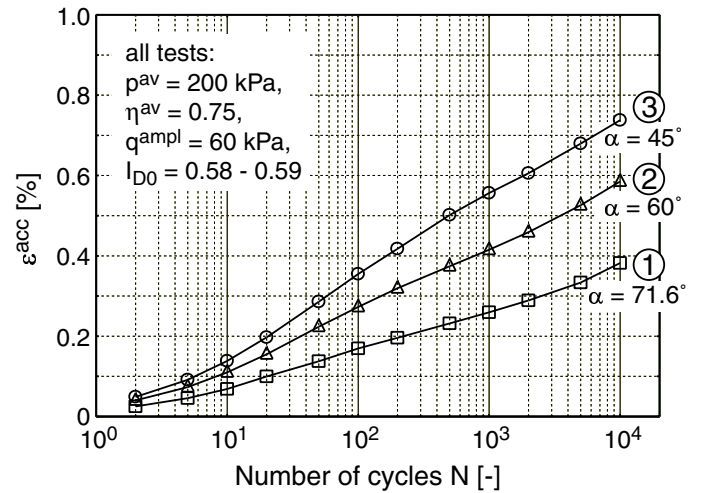


Figure 3. Accumulation of strain ϵ^{acc} with the number of cycles N in tests with an identical deviatoric but different volumetric portions of the cyclic stress path

Figure 2 presents the resulting strain loops in the $\epsilon_q - \epsilon_v$ - plane. Decreasing α and holding q^{ampl} constant means a significant increase of the volumetric portion of the strain loop ϵ_v^{ampl} , while the deviatoric part ϵ_q^{ampl} slightly decreases. If only the deviatoric part of the strain loop causes strain accumulation test No. 1 (see Fig. 1) with the highest value of ϵ_q^{ampl} should provide the highest accumulation rates. However, the curves $\epsilon^{\text{acc}}(N)$ in Figure 3 show the opposite. In the test with $\alpha = 45^\circ$ the accumulation rate was approximately twice as high as with a stress path inclined under $\alpha = 71.6^\circ$, although the deviatoric amplitude ϵ_q^{ampl} was nearly twice lower in the former case. Thus, the accumulation does depend on the volumetric portion of the strain loop.

Figure 4 presents the ratio ω of the residual volumetric and deviatoric strains as a function of the number of cycles N . Evidently the direction of accumulation turns out to be rather insensitive to the inclination of stress or strain path.

2.2 Tests with pure isotropic stress loops

Following the previous results one may ask if purely

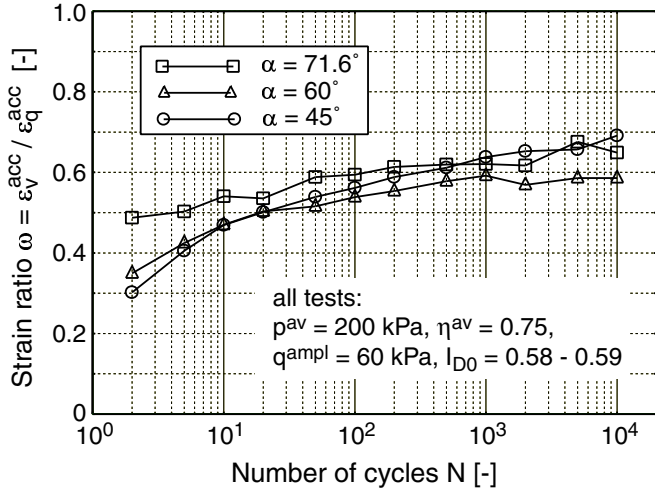


Figure 4. Strain ratio $\omega = \varepsilon_v^{\text{acc}} / \varepsilon_q^{\text{acc}}$ as a function of the number of cycles N in tests with identical deviatoric but different volumetric part of the cyclic stress path

isotropic stress or strain loops also produce deformation accumulation. Such stress loops ($q^{\text{ampl}} = 0$) with a constant amplitude $p^{\text{ampl}} = 50$ kPa were applied to specimens ($0.58 \leq I_{D0} \leq 0.61$) at $p^{\text{av}} = 200$ kPa but with four different average stress ratios η^{av} ($0 \leq \eta^{\text{av}} \leq 0.75$). The corresponding stress paths are presented in Figure 5.

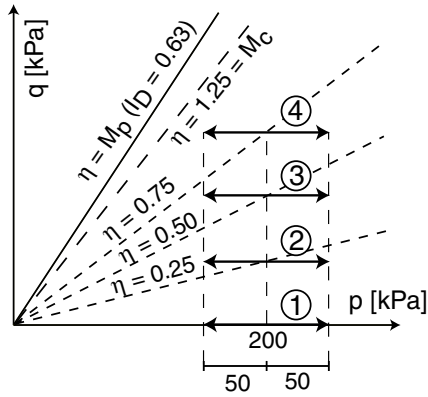


Figure 5. Stress paths in the p - q - plane in tests with a pure isotropic stress amplitude

The resulting strain loops in the ε_q - ε_v plane are shown in Figure 6. They were pure volumetric for σ^{av} lying on the p - axis. With increasing $\eta^{\text{av}} > 0$ the strain loops were not exactly volumetric (anisotropy of elastic stiffness) but the volumetric portion was predominant.

In Figure 7 the measured accumulated strain ε^{acc} is plotted against the number of cycles N . Although the loops were volumetric a significant accumulation of strain was observed. The rate of accumulation increased with η^{av} . Even at an isotropic average stress σ^{av} the rate of accumulation did not vanish contrarily to the results reported by Ko and Scott (1967). These experiments also confirm that the influence of the volumetric part of the strain loop on accumulation *cannot* be neglected.

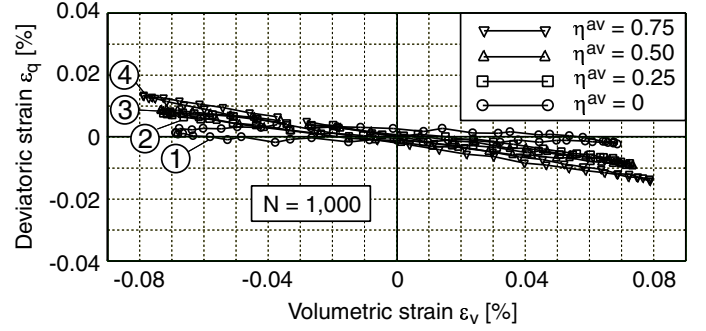


Figure 6. Strain loops in the ε_q - ε_v - plane in tests with a pure isotropic stress amplitude

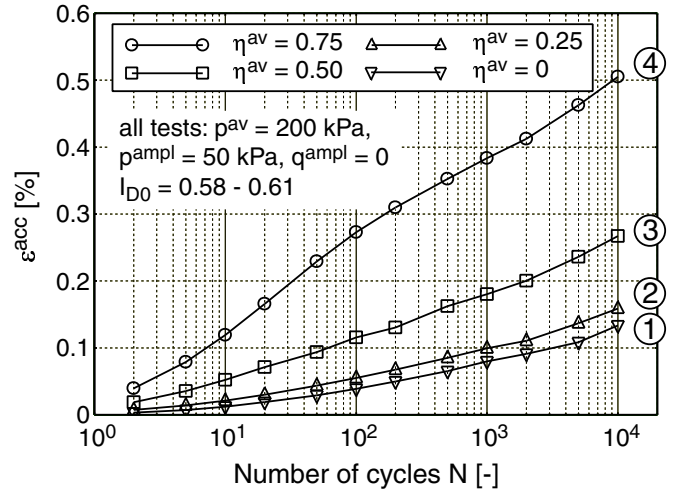


Figure 7. Accumulation of strain ε^{acc} with the number of cycles in tests with a pure isotropic stress amplitude

Figure 8 shows the accumulated strain for different cycle numbers N as a function of stress ratio \bar{Y}^{av} ($\bar{Y} = (Y - 9)/(Y_c - 9)$, $Y_c = (9 - \sin^2 \varphi)/(1 - \sin^2 \varphi)$, $Y = -I_1 I_2 / I_3$, I_i : basic invariants of stress tensor σ , φ : critical friction angle). Assuming a proportionality $\varepsilon^{\text{acc}} \sim (\varepsilon^{\text{ampl}})^2$ ($\varepsilon^{\text{ampl}} = \sqrt{(\varepsilon_P^{\text{ampl}})^2 + (\varepsilon_Q^{\text{ampl}})^2}$, see Wichtmann et al. 2004) the accumulated strain was normalized dividing by $f_{\text{ampl}} = (\varepsilon^{\text{ampl}} / \varepsilon_{\text{ref}}^{\text{ampl}})$. Fitting the function $f_Y = \exp(C_Y \bar{Y}^{\text{av}})$ (see Wichtmann et al. 2004) to the data points in Figure 8 a material constant $C_Y = 2.75$ for up to $N = 10,000$ is obtained. This material constant is slightly higher than $C_Y = 2.05$ found for stress paths with $\sigma_3 = \text{const.}$ as presented in Wichtmann et al. (2004). It can be stated that the dependence of accumulation on average stress σ^{av} is relatively insensitive to the polarization of the strain amplitude.

In Figure 9 the strain ratio ω is plotted versus the average stress ratio η^{av} . As in the tests with $\sigma_3 = \text{const.}$ documented in Wichtmann et al. (2004) the accumulation becomes more deviatoric with increasing average stress ratio η^{av} . As in the tests with $\sigma_3 = \text{const.}$ the direction of accumulation could be fitted by the flow rule predicted by monotonic constitutive models (modified Cam-clay model, hypoplastic K-model). Thus, this test series confirms that the

direction of accumulation is insensitive to the orientation of the stress path.

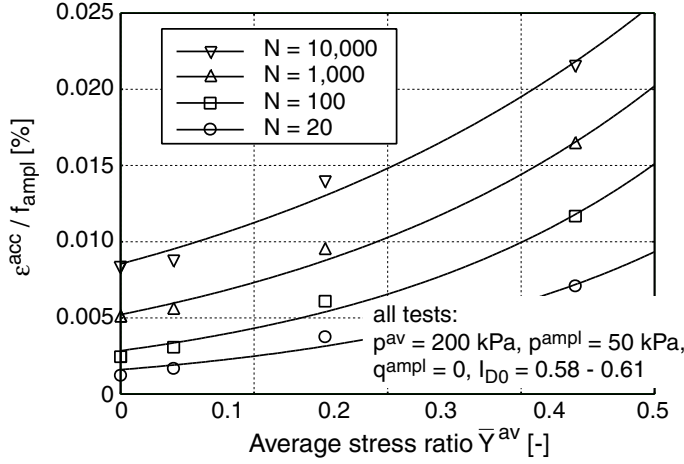


Figure 8. Accumulated strain ε^{acc} normalized by strain amplitude $\varepsilon^{\text{ampl}}$ in dependence of the average stress ratio \bar{Y}^{av} for tests with a pure isotropic stress amplitude

inclinations $\alpha = 0^\circ$. As mentioned in Subsection 2.2 isotropic stress paths produced some amount of deviatoric strain amplitude but the volumetric part of these strain loops was prevailing. Stress paths with $\alpha = 80^\circ$ (due to anisotropy of stiffness not at $\alpha = 90^\circ$) resulted in nearly pure deviatoric strain loops. Different amplitudes p^{ampl} and q^{ampl} , respectively were applied leading to the stress paths shown in Figure 10. The corresponding strain loops in the $\varepsilon_q - \varepsilon_v$ plane are presented in Figure 11.

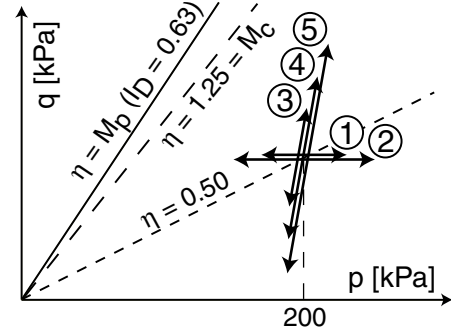


Figure 10. Stress paths in the $p - q$ - plane in tests with pure volumetric or pure deviatoric strain loops

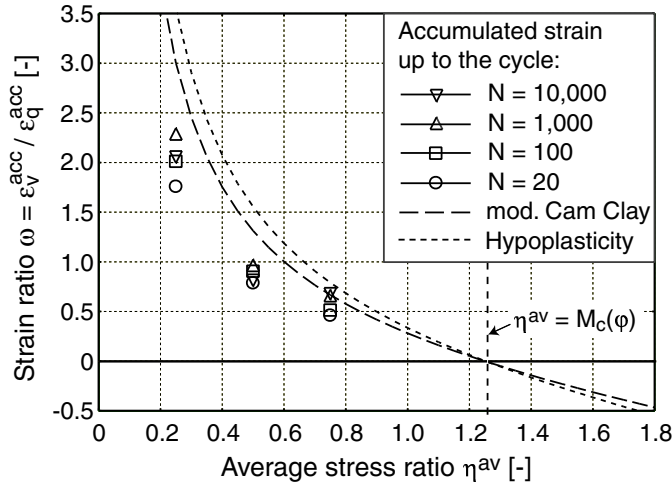


Figure 9. Strain ratio $\omega = \varepsilon_v^{\text{acc}} / \varepsilon_q^{\text{acc}}$ as a function of stress ratio $\eta^{\text{av}} = q^{\text{av}} / p^{\text{av}}$ for tests with a pure isotropic stress amplitude

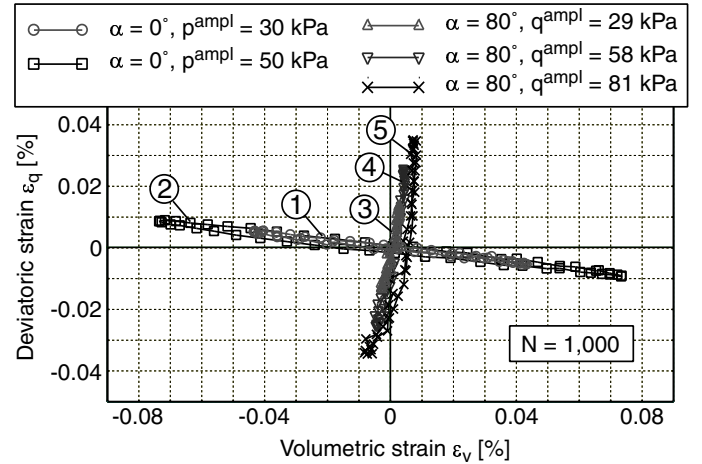


Figure 11. Strain loops in the $\varepsilon_q - \varepsilon_v$ - plane for tests with pure volumetric or pure deviatoric strain loops

2.3 Tests comparing pure volumetric and pure deviatoric strain paths of identical amplitude $\varepsilon^{\text{ampl}}$

Although we have shown that the volumetric portion of the strain amplitude contributes significantly to the rate of accumulation the question remains if the volumetric portion has an equal influence on accumulation as the deviatoric one.

In order to quantify the differences in the accumulation rates due to pure volumetric ($\varepsilon_q^{\text{ampl}} = 0$) and pure deviatoric ($\varepsilon_v^{\text{ampl}} = 0$) strain paths of equal norm $\varepsilon^{\text{ampl}} = \sqrt{(\varepsilon_p^{\text{ampl}})^2 + (\varepsilon_q^{\text{ampl}})^2} = \text{const.}$ a third series of tests was performed. The average stress was kept constant at $p^{\text{av}} = 200$ kPa and $\eta^{\text{av}} = 0.50$ and the specimens were prepared with $0.56 \leq I_{D0} \leq 0.61$. The volumetric strain loops were produced with stress paths

In Figure 12 the cumulative strain ε^{acc} is plotted versus the number of cycles. It is evident that the deviatoric strain paths produce a higher accumulation than the volumetric strain loops. This can also be seen in Figure 13, where the residual strain after 10,000 cycles is presented as a function of the strain amplitude $\varepsilon^{\text{ampl}}$. For both polarizations of the strain loop a relationship $\varepsilon^{\text{acc}} \sim (\varepsilon^{\text{ampl}})^2$ was obtained (solid and dashed curves in Fig. 13), confirming our earlier observation that the accumulation rate depends on the square of the strain amplitude. However, an identical total strain amplitude $\varepsilon^{\text{ampl}}$ may lead to different accumulation rates. The pure deviatoric strain loops produce 3.4 times higher accumulation rates compared with volumetric ones. Thus, the total amplitude $\varepsilon^{\text{ampl}}$

alone is not able to capture the accumulation rates, the contribution of the volumetric and deviatoric portions to $\varepsilon^{\text{ampl}}$ have to be considered separately.

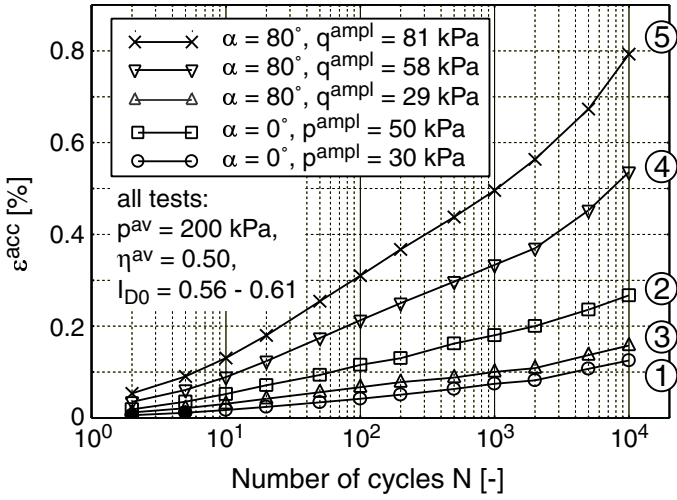


Figure 12. Curves $\varepsilon^{\text{acc}}(N)$ in tests with pure volumetric or pure deviatoric strain loops

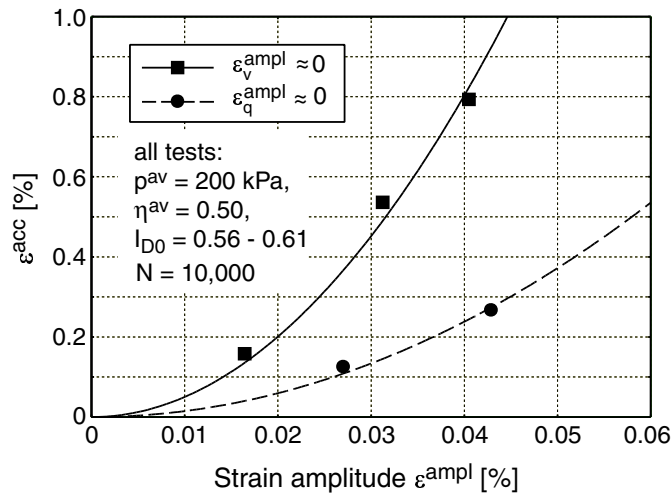


Figure 13. Accumulated strain ε^{acc} as a function of strain amplitude $\varepsilon^{\text{ampl}}$, tests with pure volumetric or pure deviatoric strain loops

The observed effect could be captured by a modification of the amplitude function f_{ampl} of the explicit constitutive model (see Section 3 of Wichtmann et al. 2004) treating the deviatoric and volumetric portions of the strain amplitude separately:

$$f_{\text{ampl}} = \left(\frac{\varepsilon_Q^{\text{ampl}} + C_{\text{ampl}} \varepsilon_P^{\text{ampl}}}{\varepsilon_{\text{ref}}^{\text{ampl}}} \right)^2 \quad (1)$$

With $\varepsilon^{\text{acc}}(\varepsilon_P^{\text{ampl}} = 0) / \varepsilon^{\text{acc}}(\varepsilon_Q^{\text{ampl}} = 0) = 3.4$ a material constant $C_{\text{ampl}} = 0.54$ is obtained. Intermediate cases with different α s will be tested in future in order to prove or disprove Equation (1) and to complete the diagram in Figure 14, where the accumulated strain

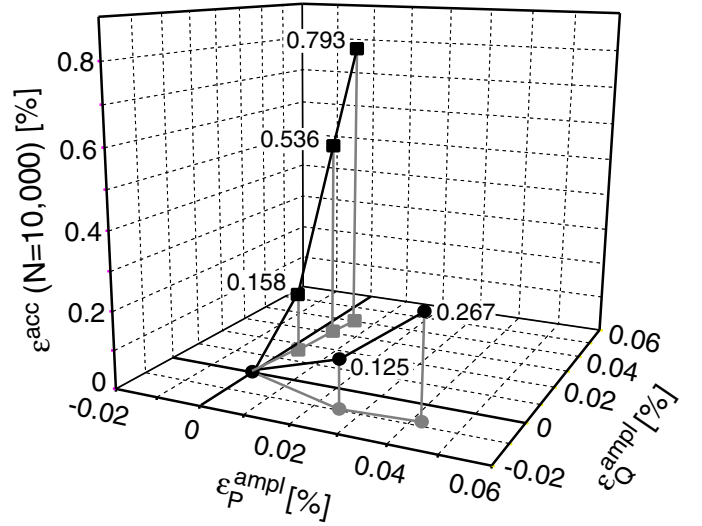


Figure 14. Accumulated strain ε^{acc} at $N = 10,000$ as a function of the volumetric and deviatoric portions of the strain amplitude

for $N = 10,000$ is plotted for different combinations of $(\varepsilon_P^{\text{ampl}}, \varepsilon_Q^{\text{ampl}})$.

The observation that the polarization and the magnitude of the strain amplitude do not influence the direction of accumulation (Fig. 15) is quite convenient in constitutive modelling.

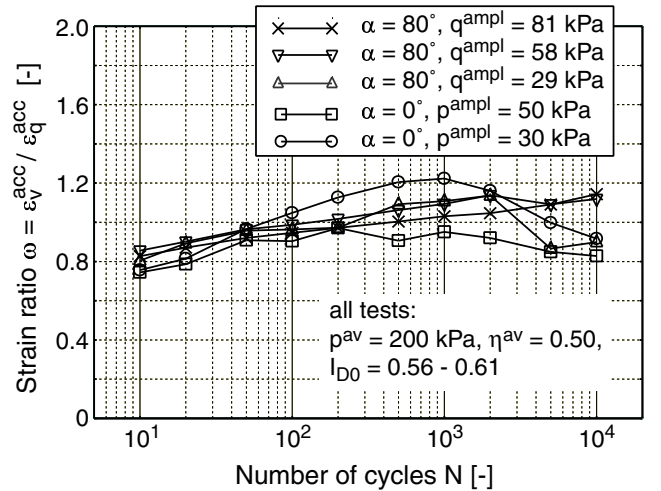


Figure 15. Strain ratio $\omega = \varepsilon_v^{\text{acc}} / \varepsilon_q^{\text{acc}}$ as a function of the number of cycles in tests with approximately pure volumetric or approximately pure deviatoric strain loops

2.4 Tests with ellipsoidal stress paths in the p - q - plane

In the fourth test series ellipsoidal stress paths in the p - q - plane (see Fig. 16) were tested. One test with a circular stress path ($p^{\text{ampl}} = 50$ kPa, $q^{\text{ampl}} = 50$ kPa) and another test with an ellipsoidal one ($p^{\text{ampl}} = 25$ kPa, $q^{\text{ampl}} = 50$ kPa) were performed so far. The average stress was $p^{\text{av}} = 200$ kPa and $\eta^{\text{av}} = 0.50$. The saturated specimens had initial densities of $0.54 \leq I_{D0} \leq 0.58$.

Figure 17 presents the generated strain loops in the

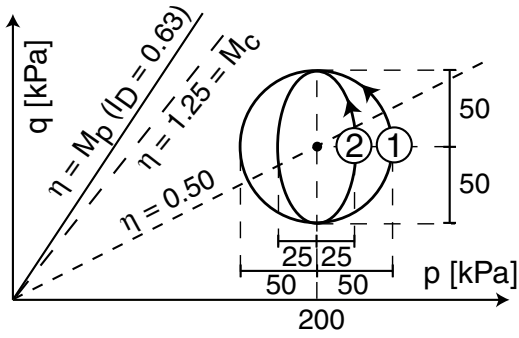


Figure 16. Ellipsoidal stress paths in the $p - q$ - plane

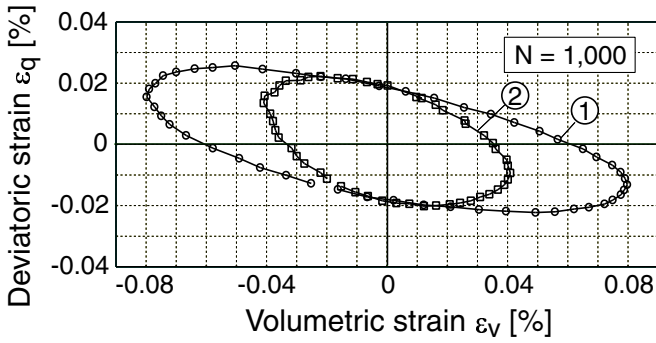


Figure 17. Strain loops in the $\varepsilon_q - \varepsilon_v$ - plane for tests with ellipsoidal stress paths in the $p - q$ - plane

$\varepsilon_q - \varepsilon_v$ - plane. The circular stress path produced strain amplitudes (amplitude = half maximum span in the ε_v - and ε_q - direction) of $\varepsilon_P^{\text{ampl}} = 0.046\%$ and $\varepsilon_Q^{\text{ampl}} = 0.031\%$. Considering Figure 13 these amplitudes would produce accumulated strains of 0.32 % and 0.50 % after 10,000 cycles if they were applied separately. Thus, a total accumulation of $\varepsilon^{\text{acc}} = 0.82\%$ would be obtained if these accumulations could simply be added without considering any interaction. As one can see from Figure 18 the combination of these amplitudes in an ellipsoidal strain path resulted in 0.70 % accumulated strain after 10,000 cycles which is slightly less than the 0.82 % mentioned above.

The ellipsoidal stress path (No. 2 referring to Fig. 16) resulted in amplitudes of $\varepsilon_P^{\text{ampl}} = 0.023\%$ and $\varepsilon_Q^{\text{ampl}} = 0.036\%$. Separately applied these amplitudes would lead to accumulated strains of 0.08 % and 0.39 % after 10,000 cycles. Thus, the total sum is 0.47 % which is identical to the value observed in the test (see Fig. 18).

However the existing test data is rare yet and several more tests with ellipsoidal stress paths in the $p - q$ - plane are necessary in order to draw meaningful conclusions and to integrate the observed effects in the constitutive model. The curves $\omega(N)$ were similar to those shown in Figure 15.

3 CYCLIC MULTIAXIAL DIRECT SIMPLE SHEAR (CMDSS) TESTS

The effect of the phase shift in multiaxial loading and

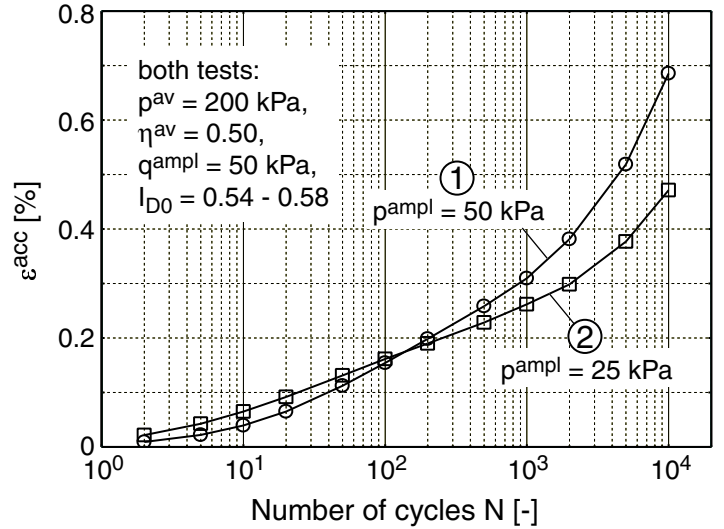


Figure 18. Accumulated strain ε^{acc} versus number of cycles N in tests with ellipsoidal stress paths in the $p - q$ - plane

the influence of a sudden change in the polarization (shearing direction) during cyclic loading was studied in a novel cyclic multiaxial direct simple shear (CMDSS) device. Two series of tests have been performed so far. In the first series the effect of a sudden rotation of the polarization by 90° was studied. The second test series compared circular (OOP) and one-dimensional (IP) strain paths.

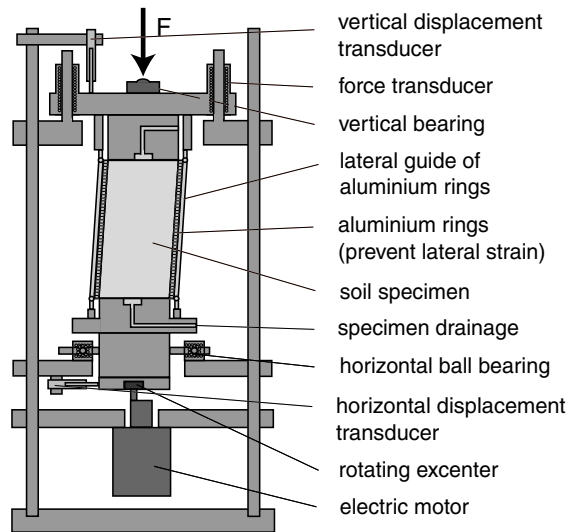


Figure 19. Scheme of the CMDSS device

Figure 19 contains a scheme of the CMDSS device, which is a modified NGI-type DSS one (see Kjellman 1951). The lower end plate of the specimen is guided by means of ball bearings in such a way that horizontal movements in arbitrary directions are possible while vertical movements are prevented. The cyclic movement of the lower end plate is caused by an electric motor driving an eccentric. The eccentric runs in a cut-out of an adapter plate, which is fixed to the bottom of the lower end plate. Different shear strain amplitudes or shapes of the strain path are achieved by using different combinations of eccentrics and slots

in the adapter plate. The upper specimen end plate is guided vertically by means of ball bearings preventing horizontal movements or tilting of this plate.

In order to obtain sufficiently small shear strains a considerable specimen height of 20 cm was chosen. The specimens have 10 cm in diameter. Lateral deformations of the specimens are prevented by means of 200 aluminium rings of 1 mm thickness, which embrace the specimen over the whole height. A membrane separates the sand and the aluminium rings. Eight extendable rods guide the aluminium rings during cyclic shearing which should guarantee a homogenous decrease of the boundary displacements with the specimen height. The rods are fixed with ball joints to the lower and upper specimen end plates.

A small vertical stress σ_1 is applied by weights on the vertically guided upper end plate, higher stresses can be obtained by using a pneumatic loading system. Since lateral strains are prevented the application of σ_1 leads to a K_0 state of stress (K_0 : earth pressure coefficient at rest).

The vertical deformation of the specimen was measured by a displacement transducer. Since lateral bulging was prevented the accumulated vertical ($\varepsilon_1^{\text{acc}}$), volumetric ($\varepsilon_v^{\text{acc}}$) and total ($\varepsilon^{\text{acc}} = \|\varepsilon^{\text{acc}}\|$) strains are identical. The horizontal movements of the lower end plate were controlled by means of two displacement transducers arranged in orthogonal directions. The shear strain amplitude γ^{ampl} was calculated as the quotient of the amplitude of the horizontal displacement and the specimen height. Since the specimen height was reduced during cyclic shearing the shear strain amplitude was somewhat increased during a test. However, the shear strain amplitudes γ^{ampl} mentioned in the following were calculated with the initial height of the specimen. The novel device was proven to apply identical shear strain amplitudes in the two perpendicular directions resulting in similar accumulation rates.

All tests were conducted on the medium coarse sand used in the cyclic triaxial tests. Specimens were prepared by dry pluviation and tested under the air-dry condition.

3.1 Influence of a sudden change of polarization

Figure 20 presents the curves $\varepsilon^{\text{acc}}(N)$ in two tests with identical initial density. In the first test (shown as dashed line) 5,000 cycles were applied in one shearing direction. In the second test (shown as solid line) the sample was sheared in the same direction as in the first test during the first 1,000 cycles. Then the shearing direction was rotated by 90° and 4,000 cycles were continued in the new direction using the same amplitude as during the first 1,000 cycles. A significant temporary increase of the rate of accumulation

$\dot{\varepsilon}^{\text{acc}}$ was observed. This effect abated during the 1,000 cycles following the rotation of polarization. Afterwards the curves $\varepsilon^{\text{acc}}(N)$ of tests No. 1 and 2 became parallel. The change of polarization may lead to an approximately 0.5 % additional accumulation at the end of the test. These observations could be confirmed for different initial densities (Fig. 21).

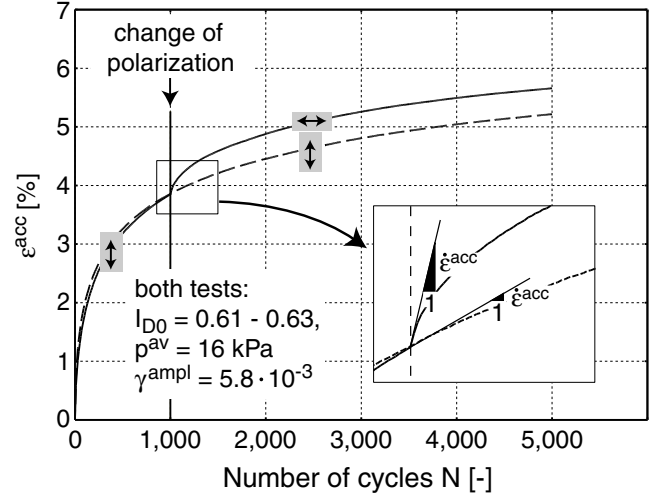


Figure 20. Increase of the accumulation rate due to a 90° rotation of shearing direction

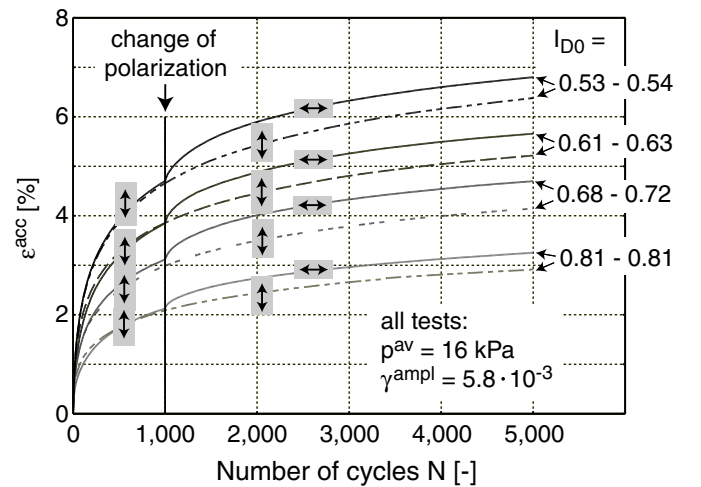


Figure 21. Increase of the accumulation rate due to a 90° rotation of shearing direction in tests with different initial densities

The explicit constitutive model introduced in Section 3 of Wichtmann et al. (2004) describes the influence of a change of the strain amplitude polarization via the partial function f_π defined as

$$f_\pi = 1 + C_{\pi 1} \left[1 - \left(\vec{\mathbf{A}}_\varepsilon :: \boldsymbol{\pi} \right)^{C_{\pi 2}} \right] \quad (2)$$

The fourth order amplitude tensor \mathbf{A}_ε is calculated from the six-dimensional strain path during a representative cycle using a series of appropriate projections. This procedure is explained in detail by Niemunis et al. (2004). The normalized amplitude tensor is

defined as polarization $\vec{\mathbf{A}}_\varepsilon$. The *back polarization* tensor π memorizes the polarization $\vec{\mathbf{A}}_\varepsilon$ during the recent cycles. Its evolution is proposed to be

$$\dot{\pi} = C_{\pi 3} (\vec{\mathbf{A}}_\varepsilon - \pi) \|\mathbf{A}_\varepsilon\|^2 \quad (3)$$

In Equations (2) and (3) $C_{\pi 1}$, $C_{\pi 2}$ and $C_{\pi 3}$ are material constants. Figure 22 illustrates schematically how the Equations (2) and (3) work. N_{cp} denotes the number of cycles at which the polarization is rotated. The polarization change causes a shift of the accumulation rate (Fig. 22a). f_π is the factor increasing the rate of accumulation due to a change of polarization. It jumps rapidly up at $N = N_{cp}$ and then it gradually declines towards 1 during the following cycles (Fig. 22b). The product $\vec{\mathbf{A}}_\varepsilon :: \pi$ is 1 if the actual strain polarization $\vec{\mathbf{A}}_\varepsilon$ is equal to the polarization during the recent cycles π and gets 0 when they are perpendicular. π accommodates to the new polarization during the subsequent cycles according to Equation (3) while the product $\vec{\mathbf{A}}_\varepsilon :: \pi$ increases towards 1 (Fig. 22c).

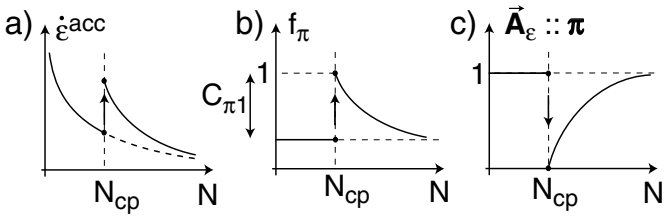


Figure 22. Capture of polarization change effects in the material model

In the tests with different initial void ratios presented in Figure 21 the accumulation rate after a 90° change of strain polarization was found to be 4 to 6 times higher than the accumulation rates before the change. According to $f_\pi(N = N_{cp}) = 1 + C_{\pi 1}$ values between $3.05 \leq C_{\pi 1} \leq 4.95$ with a tendency to increase with initial density were determined. For the time being the material constant $C_{\pi 1}$ is set to 4.0 until further test data is available.

Integration of Equation (3) delivers

$$\pi = \vec{\mathbf{A}}_\varepsilon + (\pi_0 - \vec{\mathbf{A}}_\varepsilon) \exp[-C_{\pi 3} \|\vec{\mathbf{A}}_\varepsilon\|^2 (N - N_{cp})] \quad (4)$$

and with Equation (2)

$$1 - \frac{f_\pi - 1}{C_{\pi 1}} = \left\{ 1 - \exp[-C_{\pi 3} \|\mathbf{A}_\varepsilon\|^2 (N - N_{cp})] \right\}^{C_{\pi 2}} \quad (5)$$

is obtained. In Figure 23 the curves $1 - (f_\pi - 1)/C_{\pi 1}$ resulting from the tests documented in Figure 21 are plotted versus the number of cycles after the change of strain polarization $N - N_{cp}$. The abatement of f_π for $N > N_{cp}$ was found to be almost identical for the four tested initial densities. Equation (5) was fitted to the evanescent curves resulting in $C_{\pi 3} \|\mathbf{A}_\varepsilon\|^2 = 0.006$ and $C_{\pi 2} = 0.5$.

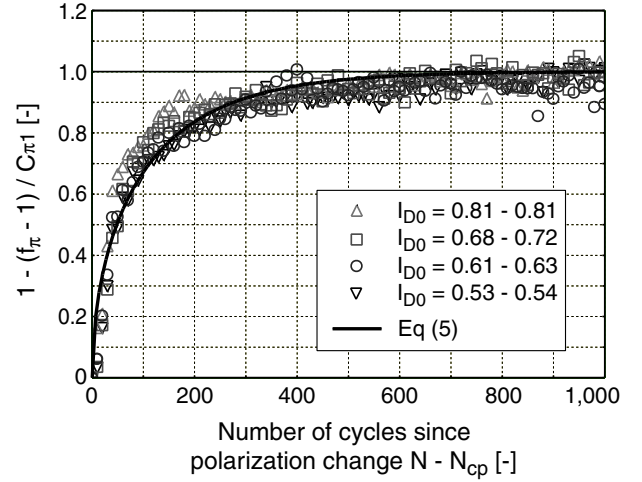


Figure 23. Abatement curves in four tests with different initial densities

3.2 Influence of the encompassed area of the strain path

The CMDSS device was also used to investigate the influence of the shape of the strain path during a cycle on the accumulation rate. Circular (OOP) and one-dimensional (IP) strain paths with identical amplitudes (i.e. identical maximum shear strains in the direction of the 1-D path) were compared. In Figure 24 the curves $\varepsilon^{\text{acc}}(N)$ of two tests with similar initial density and amplitude, but different shapes of the loop are presented. It is obvious, that the circular strain path produces a higher accumulation rate compared with the 1-D path of nearly identical (if understood as a half of the span of the loop) amplitude.

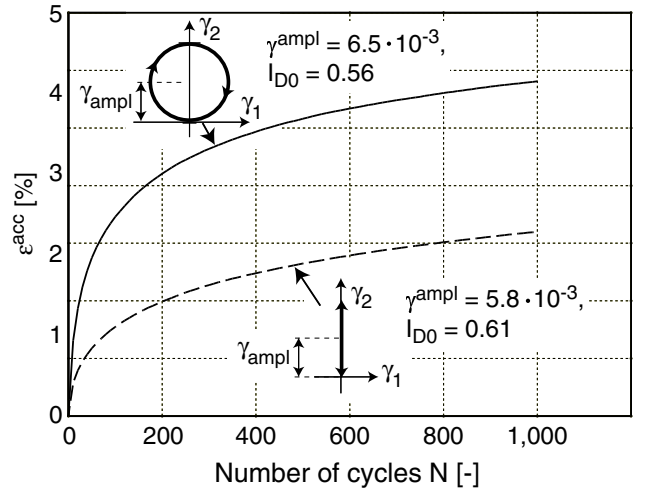


Figure 24. Accumulation due to circular and one-dimensional cyclic shearing

Data of tests with varying amplitudes is given in Figure 25 for $N = 100$. The factor between the accumulation rates of circular and 1-D paths varied between 2.2 for the smaller strain amplitudes ($\gamma^{\text{ampl}} = 1.5 \cdot 10^{-3}$) and 1.7 for the higher ones ($\gamma^{\text{ampl}} = 6.5 \cdot 10^{-3}$). Thus, it can be concluded that circular strain

paths produce approximately double accumulation compared with 1-D ones. However, it is obvious that the relation $\varepsilon^{\text{acc}} \sim (\gamma^{\text{ampl}})^2$ could not be reproduced in the CMDSS tests which is contributed to the deficits of the testing apparatus, see subsection 3.3.

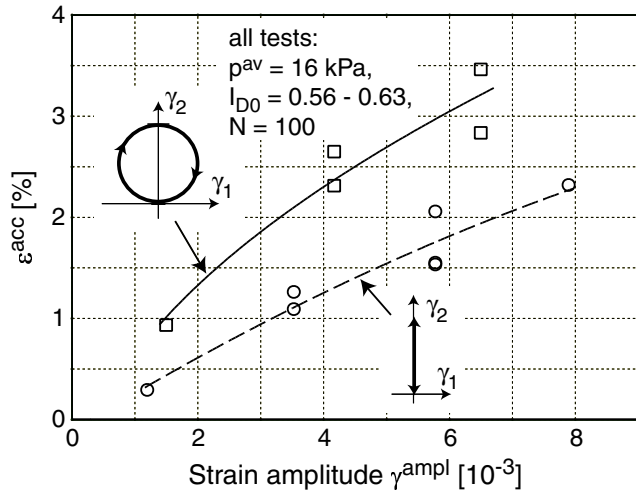


Figure 25. Influence of the shape of the strain path on accumulation in tests with different strain amplitudes

According to the definition of γ^{ampl} (see Fig. 24) and considering the definition of the multiaxial amplitude A_ε (Niemunis et al. 2004) the one-dimensional strain path leads to $\varepsilon^{\text{ampl}} = \gamma^{\text{ampl}}$ while for the circular strain path $\varepsilon^{\text{ampl}} = 1.86\gamma^{\text{ampl}}$ comes from theory. Using $\varepsilon^{\text{acc}} \sim (\varepsilon^{\text{ampl}})^2$ results in a theoretical ratio of $1.86^2 = 3.47$ of the accumulation due to circular and one-dimensional paths, respectively. The present theoretical approach delivers higher values than the experiment and thus should be modified in future.

If the sense of rotation was changed in CMDSS tests with a circular strain path from clockwise to counterclockwise, an effect of this rotation on the accumulation process was not visible (Fig. 26).

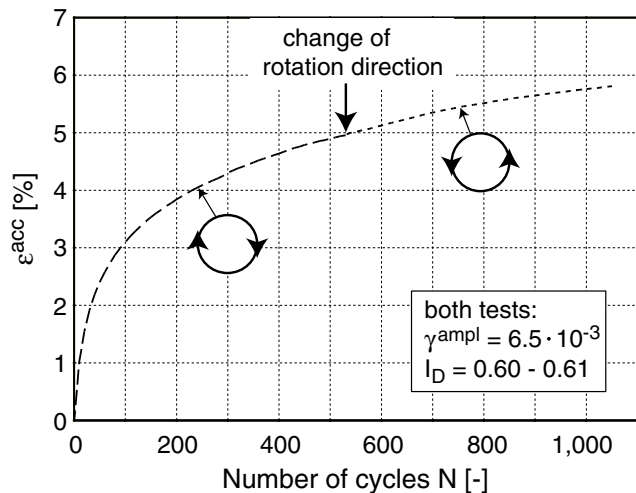


Figure 26. Effect of a change of the sense of rotation in CMDSS tests with a circular strain path

3.3 Critical remarks concerning the test device

A comparison of the accumulated strain ε^{acc} in the cyclic triaxial tests documented in Wichtmann et al. (2004) and the CMDSS tests presented in this paper reveals significantly slower accumulation rates in the CMDSS case. This can be mainly attributed to a non-uniform distribution of the shear strains and thus to a non-uniform accumulation of strain over the specimen volume. The non-uniform distribution of strain in direct simple shear tests was reported in the literature several times (e.g. Budhu 1984).

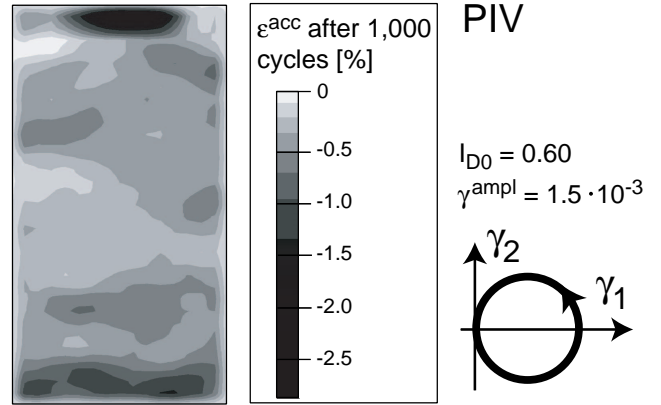


Figure 27. Distribution of accumulated strain over the specimen volume after 1,000 cycles with a circular strain path determined by PIV

The crucial problem is the friction between the rubber membrane and the aluminium rings. The friction considerably hampers the accumulation on one hand but on the other hand it seems indispensable for even distribution of strain over the height. Here we show what would happen if one smeared the aluminium rings from the inside to minimize the friction. In order to make our demonstration more blatant we remove the aluminium rings completely (= perfect smearing). The inhomogeneities were confirmed for a CMDSS test with a circular strain path ($\gamma^{\text{ampl}} = 1.75 \cdot 10^{-3}$) using the Particle Image Velocimetry (PIV) method. The specimen membrane was speckled with color spots (so-called seeding in PIV jargon). A vacuum suction of 15 kPa stabilized the specimen. The pictures of the specimen taken before cyclic loading and after 1,000 cycles were compared by a computer program leading to a strain field as presented in Figure 27. It is obvious that the strain accumulation concentrates at the ends of the specimen. A three-dimensional finite element (FE) calculation using the hypoplastic K-model confirmed that the reason for this non-uniformity of strain accumulation is a non-uniform distribution of the shear strain amplitude.

4 SUMMARY AND CONCLUSIONS

The contribution of the deviatoric and the volumet-

ric portion of the strain loop during one cycle to the accumulation rate under cyclic loading was studied in cyclic triaxial tests with a simultaneous variation of the vertical and lateral stresses σ_1 and σ_3 , respectively. Moreover cyclic multiaxial direct simple shear (CMDSS) tests were performed in order to observe the influence of the shape of the strain path and the effect of sudden changes in strain polarization on the accumulation rate. The main conclusions from these tests are:

- The volumetric part of the strain amplitude significantly contributes to the accumulation rate.
- Pure volumetric strain loops (with zero deviatoric strain amplitude) lead to a non-negligible accumulation.
- The function f_Y determined from tests with $\sigma_3 = \text{const.}$ is also valid for pure volumetric strain loops at varying average stress ratio η^{av} .
- Pure deviatoric strain loops produce approximately 3.4 times larger accumulation rates compared with pure volumetric strain loops of identical total amplitude $\varepsilon^{\text{ampl}} = \sqrt{(\varepsilon_P^{\text{ampl}})^2 + (\varepsilon_Q^{\text{ampl}})^2}$. Thus, the total amplitude $\varepsilon^{\text{ampl}}$ alone is insufficient to predict the accumulation rate.
- The accumulation due to ellipsoidal strain paths in the $\varepsilon_v^{\text{ampl}} - \varepsilon_q^{\text{ampl}}$ - plane is nearly identical with the sum of the accumulations that are generated if the volumetric and deviatoric amplitudes are applied separately. However, this conclusion is based on few test data so far and has to be confirmed in future.
- The direction of accumulation is independent of the polarization of the strain path, i.e. it depends only on η^{av} and not on the cyclic strain path around σ^{av} .
- A sudden rotation of the strain polarization causes a significant temporary increase of the accumulation rate (approximately factor 4 - 5 directly after the polarization change). This effect abates during the following 1,000 cycles.
- A circular cyclic shearing produces approximately double accumulation of strain compared with one-dimensional strain paths of identical strain amplitude.

A modification of the amplitude function f_{ampl} of our explicit constitutive model (see Section 3 in Wichtmann et al. 2004) was proposed taking into account the different contributions of the deviatoric and the volumetric portion of the strain loop to the accumulation rate. The fourth order amplitude tensor \mathbf{A}_ε capturing multiaxial strain paths and the *back polarization* tensor π memorizing strain polarization during the recent cycles were introduced. The partial

function f_π and the evolution equation of π were presented describing the effects of polarization changes during cyclic loading.

5 ACKNOWLEDGEMENTS

The authors are grateful to DFG (German Research Council) for the financial support. This study is a part of the project A8 "Influence of the fabric changes in soil on the lifetime of structures" of SFB 398 "Lifetime oriented design concepts".

REFERENCES

- Boulanger, R.W. & Seed, R.B. 1995. Liquefaction of sand under bidirectional monotonic and cyclic loading. *Journal of Geotechnical Engineering* 121(12): 870-878.
- Budhu, M. 1984. Nonuniformities imposed by simple shear apparatus. *Canadian Geotechnical Journal* 20: 125-137.
- Ishihara, K. & Yamazaki, F. 1980. Cyclic simple shear tests on saturated sand in multi-directional loading. *Soils & Foundations* 20(1): 45-59.
- Kjellman, W. 1951. Testing the shear strength of clay in Sweden. *Géotechnique* 2(3): 225-232.
- Ko, H.Y. & Scott, R.F. 1967. Deformation of sand in hydrostatic compression. *Journal of the Soil Mechanics and Foundations Division* 93(SM3): 137-156.
- Niemunis, A. 2003. Extended hypoplastic models for soils. Report No. 34, Institute of Soil Mechanics and Foundation Engineering, Ruhr-University Bochum.
- Niemunis, A., Wichtmann, T. & Triantafyllidis, Th. 2003. Compaction of freshly pluviated granulates under uniaxial and multiaxial cyclic loading. In *XIIIth European Conference On Soil Mechanics and Geotechnical Engineering: Geotechnical problems with man-made and man-influenced grounds*, Prag: 855-860.
- Niemunis, A., Wichtmann, T. & Triantafyllidis, Th. 2004. Explicit accumulation model for cyclic loading. In *International Conference on Cyclic Behaviour of Soils and Liquefaction Phenomena, Bochum, 31 March - 02 April*. Balkema.
- Pyke, R., Seed, H.B. & Chan, C.K. 1975. Settlement of sands under multidirectional shaking. *Journal of the Geotechnical Engineering Division* 101(GT4): 379-398.
- Seed, H.B., Pyke, R.M. & Martin, G.R. 1978. Effect of multidirectional shaking on pore pressure development in sands. *Journal of the Geotechnical Engineering Division* 104(GT4): 27-44.
- Wichtmann, T., Niemunis, A. & Triantafyllidis, Th. 2004. Strain accumulation in sand due to drained uniaxial cyclic loading. In *International Conference on Cyclic Behaviour of Soils and Liquefaction Phenomena, Bochum, 31 March - 02 April*. Balkema.
- Yamada, Y. & Ishihara, K. 1982. Yielding of loose sand in three-dimensional stress conditions. *Soils & Foundations* 22(3): 15-31.